Compact field-deployable automated c-axis analyzer for ice thin sections

Merlin L. MAH,[1] Wing S. CHAN,[1*] Dave A. HULTMAN,[1†] Joan J. FITZPATRICK,[2] Donald E. VOIGHT,[3] Joseph J. TALGHADER[1]

[1]*Dept. of Electrical & Computer Engineering, University of Minnesota, Minneapolis, MN, USA*

[2]*Geosciences and Environmental Change Science Center, US Geological Survey, Denver, CO, USA*

[3]*Department of Geosciences, The Pennsylvania State University, University Park, PA, USA*

Correspondence: J. J. Talghader <joey@umn.edu>

ABSTRACT. Automated c-axis analyzers are a critical tool for harvesting large-scale ice crystal orientation data from thin section analysis, but existing examples are not designed for deployment into the field. We demonstrate a possible solution to this need with the Automated Lightweight Portable Analyzer for C-Axes (ALPACA), which implements the established four-sequence measurement algorithm of Wilen (2000) using three motorized axes of motion in a unit with volume about 0.034 cubic meters. In tests of eight easily-visible grains in thin section WDC-06A 420 VTS, ALPACA's polarizer rotation angles of extinction agreed with previously published data to within 5° on all but one sequence of a single grain, with average sequence errors of 1.6°, 1.3°, 1.4°, and 2.9°. The information produced by these automated measurements enable production of complete grain-by-grain orientation data.

INTRODUCTION

The thin section analysis of ice has long been a mainstay of glaciology. Glacier ice is a polycrystalline matrix of ice Ih, the only naturally occurring ice crystal structure at temperatures and pressures seen near the surface of the earth. These ice Ih crystals have a hexagonal crystal structure (thus the 'h' in Ih)

*Present address: Intel Corp., Hillsboro, OR, USA
†Present address: GE Power & Water, Minneapolis, MN, USA

with the c-axis, perpendicular to the hexagonal planes, having a lattice spacing larger than that in-plane. Each crystal has a c-axis orientation and a size usually in the range of a millimeter to a few centimeters (see, e.g., Petrenko and Whitworth (1999)). The statistics of the crystal size and orientation, collectively known as fabric, contain information on environmental variables such as—to cite just a few workers—deposition rates (Paterson and Waddington (1984)), temperature (Petit and others (1987)), flow history (Rigsby (1960), Pettit and others (2007)), and microscopic information on bubble density and dissolved or insoluble impurities (Diprinzio and others (2005), Durand and others (2006)). Despite the best efforts of remote-sensing and borehole probes (Gow and Kohnen (1979), Doake and others (2002), Matsuoka and others (2009), Gusmeroli and others (2012), Kluskiewicz and others (2017)), thin section analysis remains the only way to obtain large scale statistics of grain-level data on ice crystal orientation. Contemporary projects such as EastGRIP still produce and analyze thin sections even as drilling progresses, analyzing their crystal orientations in the field with manually-operated universal stages (personal communication with R. M. Nunn, 2019.)

Of course, this process has not escaped the drive towards automation. An automated c-axis analysis system described by Wilen (2000), housed at Pennsylvania State University, has become a mainstay of U.S. glaciological research. Several other automated analysis systems worldwide have been constructed specifically for ice thin section analysis; a selection is reviewed by Wilen and others (2003). Petrographic microscopes equipped for polarization analysis are common equipment in other areas of geology. (Fueten (1997), Wilson and Peternell (2011)) However, glaciological research is by necessity a highly itinerant activity, as the samples of interest can only be found in relatively inhospitable locations and are very prone to melting if handled in conditions compatible with human comfort. Retrieving and transporting ice cores to domestic research facilities is an extremely long and expensive undertaking. (Slawny and others (2014)) Almost all existing automated c-axis analyzers designed without regards for field deployment, so thin section analysis requires manual Rigsby stages, which are labor-intensive, time consuming, and uncomfortable to operate in cold-climate field work.

We describe the implementation and first tests of an automated, highly-portable system for c-axis analysis, whimsically dubbed the Automated Lightweight Portable Analyzer for C-Axes (ALPACA). It uses a modified implementation of the established Rigsby stage and the Wilen measurement procedure Wilen (2000) to reduce mechanical complexity and device footprint. The ALPACA mechanisms are designed to be transport-ready with outer dimensions of 12 $\times$ 12 $\times$ 14 inches, and able with minimal setup to operate

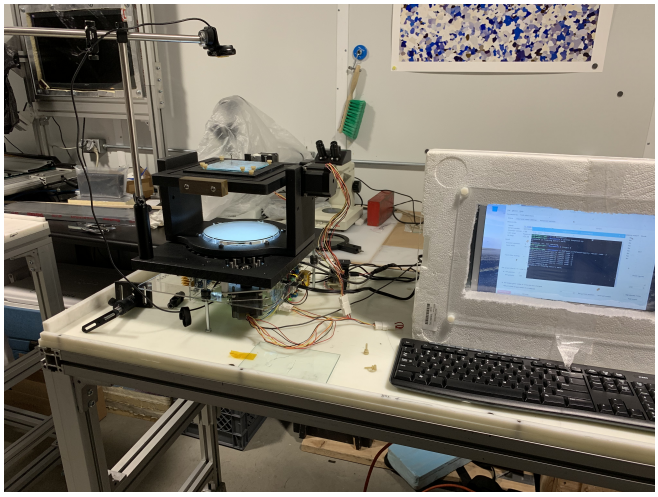

(a) Testing at ICF, July 2019

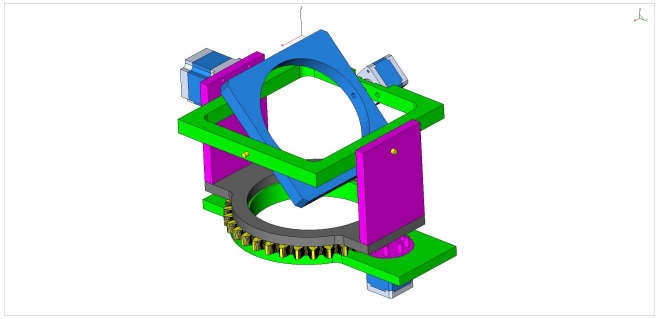

(b) CAD model

Fig. 1. (a) Photo of the stage prototype during tests at the National Science Foundation Ice Core Facility in July 2019. All motor drivers and electronics boards required by ALPACA are mounted underneath it, exposed to the -24°C air; the insulated box to the right houses a portable computer monitor and AC/DC adapters, the latter more to heat the monitor than for their own benefit. (b) A CAD model of the ALPACA stage.

in a space not much larger.

CONCEPT

In the inaugural publication Wilen (2000) of his automated c-axis analyzer, Wilen describes a procedure of four motion sequences used to obtain a c-axis reading. Each of the four sequences consists of orienting the thin section in a fixed position with respect to the laboratory frame and camera, taking a series of images while rotating the crossed polarizers which bracket the sample in the optical path, and extrapolating polarizer rotation angle at which the light transmission of each crystal reaches extinction (minimum). The stationary system built by Wilen to execute this algorithm comprises five motion stages: two tilt and one

inner rotation stage to position the sample, and two rotation stages for the polarizers bookending it.

In concept, the primary spatial relationship is that between the polarizers and the ice sample; it makes no difference whether we achieve the rotation of the light polarization by rotating both polarizers bracketing the sample, or by rotating the sample between the two static polarizers. Authors such as Fueten (1997) have made valid points about the convenience of the former approach, as it leaves the sample's position unchanged relative to the camera and thus eases image interpretation. However, this luxury requires two sets of drive mechanisms, with an attendant doubling of complexity, fragility, and cost. For a system prioritizing size and weight, we should therefore prefer to rotate the stage about the optic (fixed z) axis.

These three-dimensional stage positions can be expressed as 3x3 rotation matrices. We will here adopt the same notation as Wilen, a blend of geological and kinematics conventions, for our discussion of spatial terms. If looking downward upon a four-point compass overlaid on the thin section, the y-direction will be to the North, the positive x-direction will lie to the East, and the camera or observer will be perched at the positive end of the z-axis. Angles of rotation about each axis will have sign as determined by the right-hand rule. The rotation matrices about the x-, y-, and z- axes are expressed respectively by

$$
\begin{aligned}
R_x(\gamma) &= \begin{bmatrix} 1 & 0 & 0 \\ 0 & \cos\gamma & -\sin\gamma \\ 0 & \sin\gamma & \cos\gamma \end{bmatrix} \\
R_y(\xi) &= \begin{bmatrix} \cos\xi & 0 & \sin\xi \\ 0 & 1 & 0 \\ -\sin\xi & 0 & \cos\xi \end{bmatrix} \\
R_z(\phi) &= \begin{bmatrix} \cos\phi & -\sin\phi & 0 \\ \sin\phi & \cos\phi & 0 \\ 0 & 0 & 1 \end{bmatrix}
\end{aligned}
\tag{1}
$$

The same matrices serve rotations about fixed and Eulerian (moving, i.e., each transformation repositions the axes for subsequent steps) axes, with the distinction made by the order of their application. Craig (2005)

To begin sequence 1, the thin section lies flat, normal to the optical chief ray. This requires no motion

from the intuitive starting position of the thin section, so its kinematics frame ${}^{seq1}P$ remains identical to the universal or camera polarizer (analyzer) frame. Sequence 2 requires a 45° tilt about the y- (North-South) axis, a single rotation $R_y(\xi = 45°)$. Sequence 3 does the same (after restarting at the initial position) about the x- (East-West) axis, giving $R_x(\gamma = 45°)$. It is evident by observation that these sequences can be handled with either two orthogonal tilt stages, by rotating a single tilt stage, or by rotating the sample upon a single tilt stage.

Sequence 4 finally involves more than one axis. In Wilen's instrument, it is accomplished by a 45° tilt about the y-axis, followed by a -45° rotation about the now-tilted thin section normal. These two matrices evaluate to:

$$
\begin{aligned}
{}^{\text{Wilen seq 4}}_{\text{init}}R &= R_y(\xi = 45°) \cdot R'_z(\phi' = 45°) \\
&= \begin{bmatrix} \cos\xi\cos\phi & -\cos\xi\sin\phi & \sin\xi \\ \sin\phi & \cos\phi & 0 \\ -\sin\xi\cos\phi & \sin\xi\sin\phi & \cos\xi \end{bmatrix} \\
&= \begin{bmatrix} 1/2 & 1/2 & \sqrt{2}/2 \\ -\sqrt{2}/2 & \sqrt{2}/2 & 0 \\ -1/2 & -1/2 & \sqrt{2}/2 \end{bmatrix}
\end{aligned}
\tag{2}
$$

where the prime denotes a Eulerian z-rotation.

To minimize the number of motorized mechanisms required, our previous logic has led us towards the choice of two in-plane tilt axes and one encompassing rotation stage. One tilt stage—let us say the rotation-about-y stage—is mounted upon, and thus affected by, the other, which must now be the tilt that rotates the sample about x; the z stage acts upon both x and y rotation axes and is itself fixed to the universal reference frame. Thus, If utilizing all three stages in their order of appearance in this paragraph, this transformation can be expressed as

$$
\begin{aligned}
{}^{\text{ALPACA seq 4}}_{\text{init}}R &= R_z(\phi)\cdot R_x(\gamma)\cdot R_y(\xi) \\
&= \begin{bmatrix} -\sin\phi\sin\gamma\sin\xi+\cos\phi\cos\xi & -\sin\phi\cos\gamma & \sin\phi\sin\gamma\cos\xi+\cos\phi\sin\xi \\ \cos\phi\sin\gamma\sin\xi+\sin\phi\cos\xi & \cos\phi\cos\gamma & -\cos\phi\sin\gamma\cos\xi+\sin\phi\sin\xi \\ -\cos\gamma\sin\xi & \sin\gamma & \cos\gamma\cos\xi \end{bmatrix}
\end{aligned} \tag{3}
$$

Setting this matrix equal to the result of Wilen's prescribed motion about two Eulerian axes, we find that they are equivalent if

$$
\begin{aligned}
{}^{\text{ALPACA seq 4}}_{\text{init}}R &= R_y(\xi=35.26^\circ)\cdot R_x(\gamma=-30^\circ)\cdot R_z(\phi=-35.26^\circ) \\
&= R_y(\xi=45^\circ)\cdot R'_z(\phi'=45^\circ) = {}^{\text{Wilen seq 4}}_{\text{init}}R
\end{aligned} \tag{4}
$$

Since our polarizers are not able to move with respect to the universal laboratory frame (personified by the camera), the orientation of the thin section is optically equivalent to that achieved by the Wilen hardware. Further rotation of the z-axis will again have the same optical effect as synchronized rotation of motorized polarizers. Therefore, a ALPACA measurement sequence should yield the same results as on Wilen's instrument as long as the thin section's starting orientations are equivalent.

DESIGN

For the reasons outlined in the previous section, the stage implements three motorized rotations: one tilt stage, typically operated as rotation about a fixed y-axis; an "inner" tilt stage mounted on the first, typically used as rotation about a moving x-axis; and a rotation stage bearing both tilt stages, representing rotation about a fixed z-axis. Concentric within (but not in contact to) the large-diameter z rotation stage is an array of 165 low angular spread white LEDs, which emits white light upwards through a 6"-diameter diffuser and a linear polarizer. The thin section is mounted on the innermost of tilt stages via thumbscrews at the edges.

The stage mechanism is composed of black textured Delrin polymer, chosen for its ease of machining, durability, and avoidance of brittleness at low temperatures; the matte finish is intended to minimize stray light reflections. Both tilt stages are directly attached to stepper motors, as the torques required are not large. A 32-tooth spur gear cut into the outer edge of the tilt stage structure's bottom allows the azimuthal

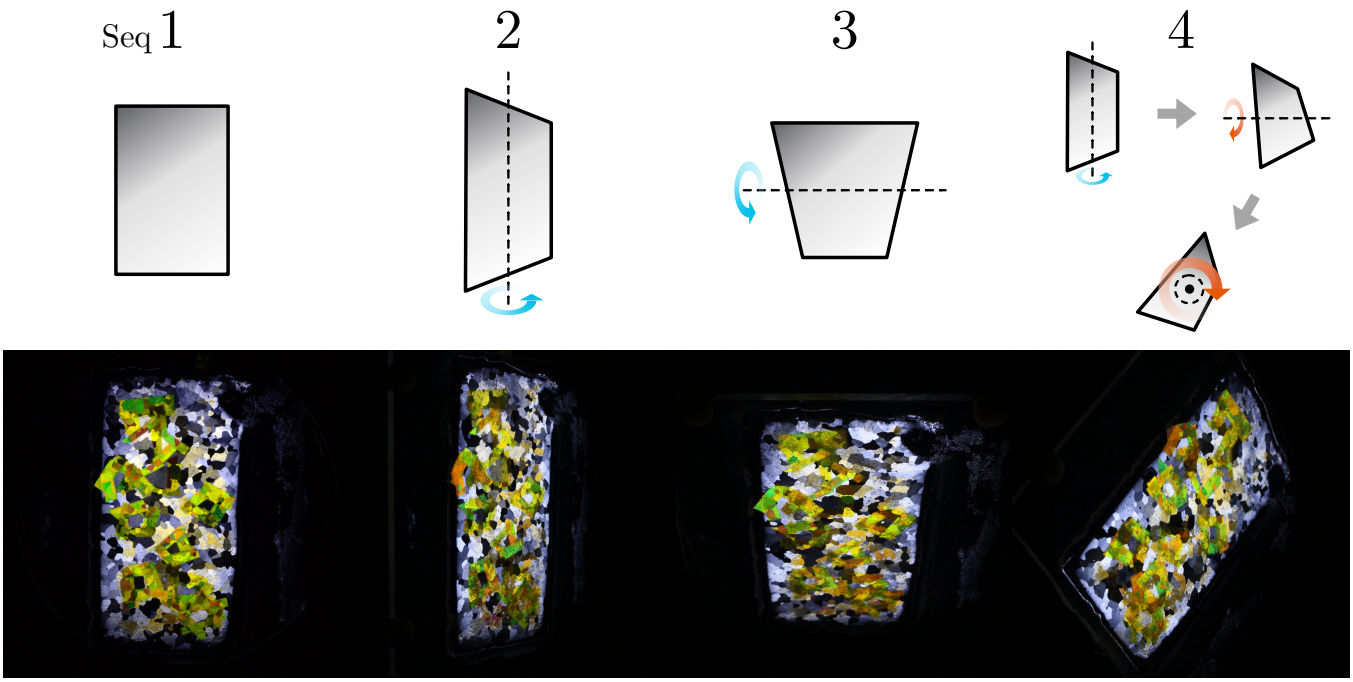

Fig. 2. Top row: Visualizations of the ice thin section's starting (0° polarizer rotation) orientation, along with the rotation axes used by the ALPACA stage to achieve this orientation, for each of the four sequences. (As a reminder, all sequences start afresh from the initial position of sequence 1.) These visualizations are exaggerated depictions of the thin section as viewed from the camera position above it; angles are not to scale. Sequence 4 shows one possible ordering of operating the three stages; the differing-color arrows indicate rotations by a negative angle, and the positive z-axis points toward the reader. Bottom row: a photo of vertical thin section WDC-06A 420 placed into the corresponding position by ALPACA.

rotation to be driven by a stepper, via 8-tooth gear, mounted outside of the lighting/optical path. The motors have been found to operate satisfactorily at -24°C without modification, although their standard lubricant may be exchanged for a low-temperature compound in the future. The full range of stage motion necessary for measurements requires only a few inches to be added to the parked stage's 12 × 12 × 14 inch outer dimensions, allowing ALPACA to be permanently mounted in a protective case for both transport and use. Operation is orchestrated by a Python script running on a Raspberry Pi single-board computer under the Raspbian operating system.

EXPERIMENT

To test the kinematics assertions above, the four-sequence procedure was performed on WDC-06A 420 VTS, a vertical thin section from the WAIS Divide ice core. This was previously measured in several published datasets. The most complete, gathered as part of a study by Fitzpatrick and others (2014) and Voigt and others (2015) of the WAIS Divide core, was obtained using the stationary Wilen system and serves as our reference data. A more recent experiment Chan and others (2014) had outlined ten easily-visible grains using Kapton tape on the glass reverse of the thin section; we left the Kapton in place as markers to aid in grain identification, although they obscured neighboring areas.

The Wilen procedure calculates the most likely c-axis orientation from the polarizer rotation angles observed to cause extinction in each of the four measurement sequences. A direct comparison of these actual observables will best evaluate the ability of our device to replicate c-axis measurement results and avoid additional complications. Following this logic, the expected extinction angles are calculated from the c-axis data of Voigt and others (2015) and compared against the same obtained by our device.

Stage positioning and polarization angle rotation were automated. At each sample orientation and polarizer angle, images were taken using a manually-triggered digital SLR camera (Canon SL1) with fixed exposure settings. In subsequent analysis, the RGB-summed intensity averaged over an 15×15 pixel area was recorded for each grain. The SURF point detection and transformation estimation function (Bay and others (2008)) was used to estimate the in-plane rotation matrices of each image relative to the preceding one and adjust the sampling coordinates to track the grains. A few millimeters of unintended translation, the result of some travel in parts of the stage, was also detected in some frames and compensated for with the same methods. The resulting data are plotted for one example grain in Figure 4, and for all eight grains in Figure 5.

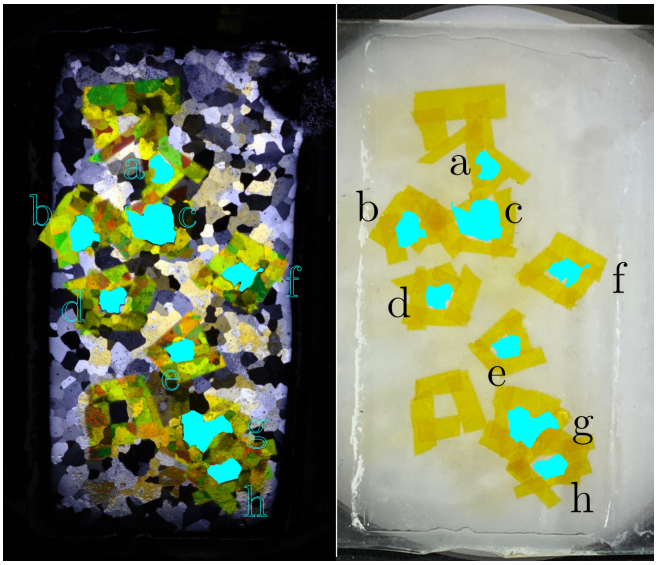

Fig. 3. Locations of the grains (shown with a solid color fill) tested within WDC-06A 420 VTS when viewed through (left) crossed polarizers at the "flat" starting orientation for sequence 1, and (right) under unpolarized lighting. Stratigraphic north is at the top of the image.

From this transmission data, a -13° offset between the crossed polarizers' transmission axis and the sample's defined $\phi = 0$ axis was uniformly subtracted from the polarization angle values. The angles of extinction were then interpolated using a three-point quadratic fit of the data point of minimum registered intensity and its two nearest neighbors. Tables 1 and 2 present the results, along with the values predicted by the reference data, and the smallest angle between the two (i.e., with integer multiples of 90° added where necessary to express the angle in the same quadrant.)

DISCUSSION

Of the ten tape-outlined grains on this thin section, two showed very large error in sequence 1, which directly measures the c-axis azimuthal angle ϕ_c, and significant error in at least two of the other three sequences. Manual checks led us to conclude that these two crystals had become re-oriented or recrystallized in the years after the reference data was collected, and thus to exclude these from our testing data. Among the remaining eight grains, ALPACA reported the extinction polarizer angles of seven to within $\pm 3.6^\circ$ of the value predicted by the traditional Wilen instrument in 31 out of 32 measurements. (Interestingly, the grain which experienced the outlier result was previously found by Chan and others (2014) to disagree with the θ_c assigned to it by Voigt and others (2015), although our observations show a larger difference with the

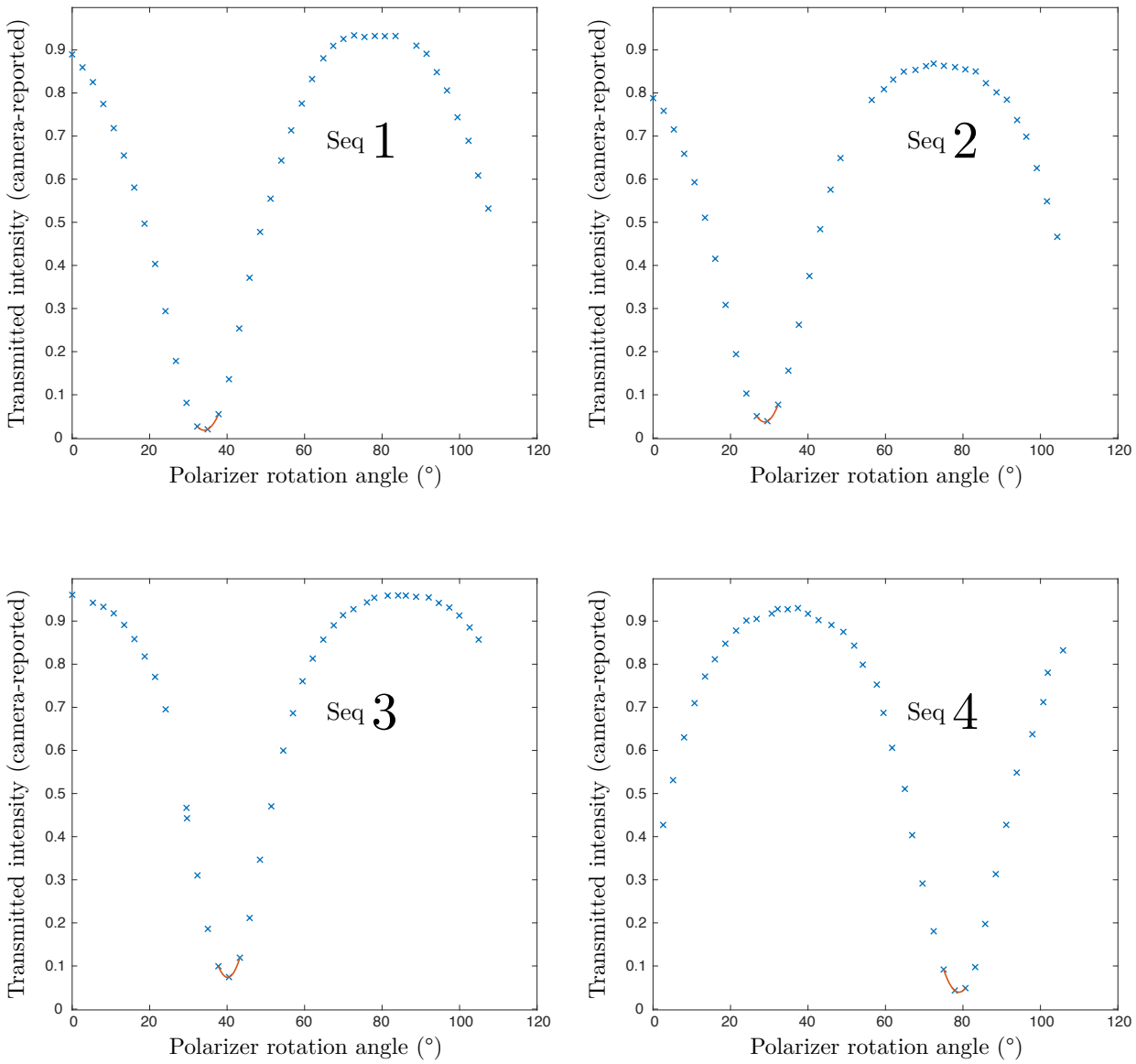

Fig. 4. Polarizer rotation angle vs. transmitted light intensity (as registered by the non-calibrated camera sensor) for grain (a) in the sequences 1, 2, 3, and 4. The red line is a quadratic fit, applied to the minimum-intensity point and its nearest neighbor to each side, used to interpolate the polarizer angle of extinction.

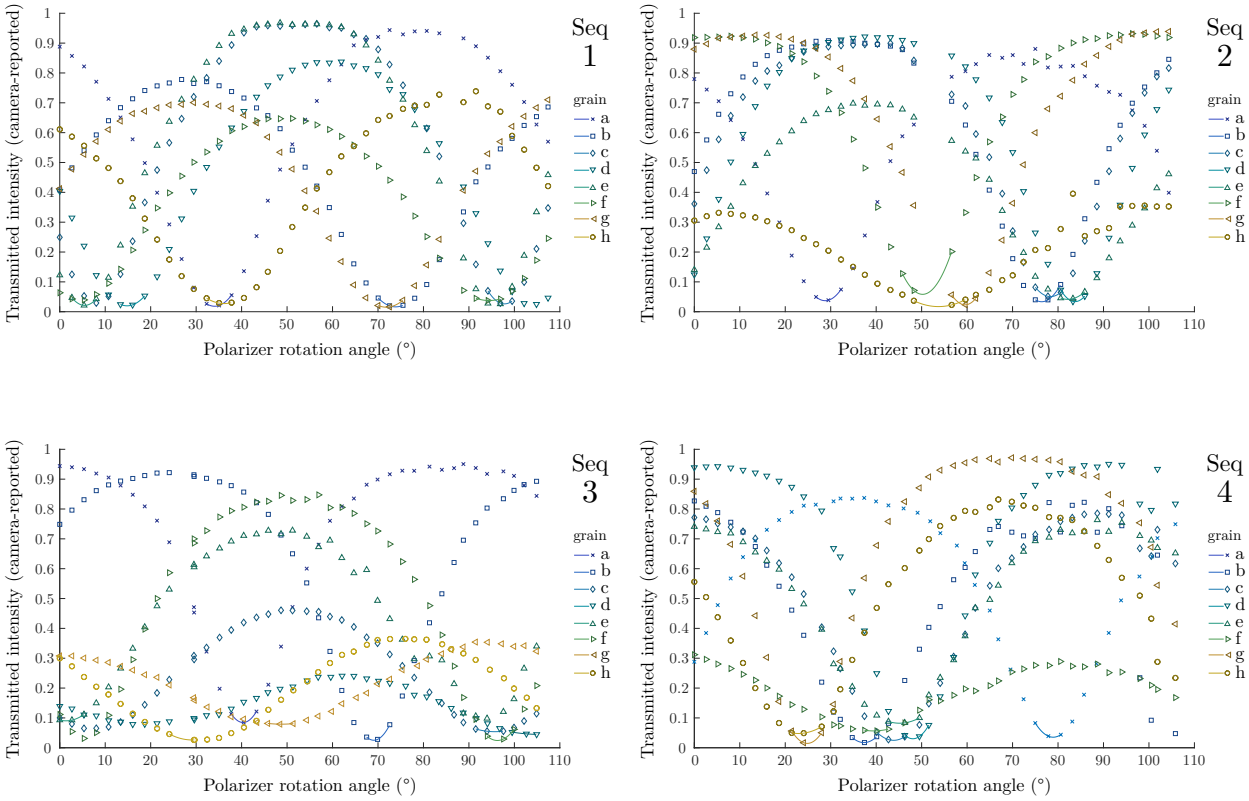

Fig. 5. Polarizer rotation angle vs. transmitted light intensity (as registered by the non-calibrated camera sensor) for each of the eight grains (a)—(h) measured in the four sequences.

Table 1. For each of the eight grains of WDC-06A 420 measured: the grain ID, c-axis elevation and azimuth results as listed by Voigt and others (2015) using the traditional Wilen system; and for sequences 1 and 2, the polarizer angles for extinction predicted by this c-axis, the polarization angle of extinction observed using the ALPACA stage, and the difference between the predicted value and the closest periodic repeat (angle plus integer multiple of 90°) of the observed value. All angles are given in degrees, with a −13° offset applied to correct an offset between the polarizers and the thin section's azimuthal $\phi = 0$ axis. The predicted, measured, and difference between polarizer angles for sequences 3 and 4 are shown separately in Table 2.

Grain label	Grain ID	θ_c	ϕ_c	Seq 1			Seq 2		
				Predicted	Measured	Difference	Predicted	Measured	Difference
a	30	−85.7	−68.7	−68.7	21.1	0.2	−74.1	15.8	0.1
b	68	69.5	−26.9	26.9	60.8	2.3	−25.4	63.4	1.2
c	60	56.6	84.7	84.7	84.8	−0.1	66.5	65.3	1.2
d	109	−58.7	−89.2	−89.2	1.9	−1.1	72.4	70.8	1.6
e	153	63.8	84.0	84.0	−7.5	1.5	70.4	69.1	1.3
f	100	−31.7	77.8	77.8	81.4	−3.6	−54.5	37.3	−1.8
g	198	54.3	62.3	62.3	58.8	3.5	48.7	46.9	1.8
h	229	47.8	−66.5	−66.5	23.2	0.3	−48.0	40.7	1.3

Table 2. Continuing from Table 1, for sequences 3 and 4: the polarizer angles for extinction predicted by the c-axis data of Voigt and others (2015), the polarization angle of extinction observed using the ALPACA stage, and the difference in polarizer angle between the predicted value and the closest periodic repeat (angle plus integer multiple of 90°) of the observed value. All angles are given in degrees.

Grain label	Seq 3			Seq 4		
	Predicted	Measured	Difference	Predicted	Measured	Difference
a	−64.0	27.0	−1.0	67.5	65.9	1.6
b	−33.2	56.1	0.7	−64.0	24.3	1.7
c	−100.8	82.7	−3.5	32.5	30.8	1.7
d	−88.4	91.8	−0.2	38.1	35.1	3.0
e	−100.4	77.5	2.1	34.4	32.1	2.3
f	−97.1	83.6	−0.7	−72.9	26.4	−9.3
g	−142.4	35.8	1.8	14.0	11.8	2.2
h	−72.5	16.1	1.4	−7.9	9.9	1.1

suggested alternative.)

The average magnitude of disagreement from predicted extinction angle among the eight grains for sequences 1, 2, 3, and 4 were 1.6°, 1.3°, 1.4°, and 2.9°, respectively. Sequence 4's notably higher error magnitudes were not wholly unexpected, given that we observed misfocus issues in some frames and that two of our three drivers are precision-limited to slightly missing the prescribed sample orientation. Tracking of sample rotation was anticipated to be a challenge and thus subjected to manual review, but very few cases were found to potentially warrant correction of the intensity readout locations.

NEXT STEPS

This prototype has demonstrated the feasibility of the compact stage design, and only a few more refinements are necessary before the ALPACA is ready for field deployment. The azimuthal/polarizer rotation mechanism was modified with relaxed tolerances to deal with a significant vertical temperature gradient which arose during testing in a chest freezer; it will be re-machined to tighter specifications and fitted with roller bearings to more gracefully eliminate this issue. This should also greatly reduce or eliminate the unintended translation previously noted in some images. The motor drivers propelling the x- and z axes will be replaced with a model (already in use on the y-axis) capable of better current control and microstepping to increase positioning precision, particularly for measurement sequence 4, and reduce waste heat. A compact digital imaging sensor and optics will be integrated with the automated measurement routine, a task that was already completed but reversed when the equipment used was discovered to gradually lose focusing ability in the cold. The stage-operation and analysis software, tested in a very rudimentary state, is slated to gain a slew of features such as a graphical user interface, automated crystal identification and coalescing, and onboard calculation of c-axis orientation. Finally, the ALPACA stage needs to be packaged into a robustly protective outer case, allowing it to venture into the field and to the rescue—one hopes—of many a glaciologist's fingertips.

ACKNOWLEDGEMENTS

M. L. Mah, W. S. Chan, and J. J. Talghader thank Richard M. Nunn and Geoff M. Hargreaves of the NSF Ice Core Facility for their hospitality and many enlightening discussions. This work was supported by the National Science Foundation under Grant 1643864.

REFERENCES

Bay H, Ess A, Tuytelaars T and Van Gool L (2008) Speeded-Up Robust Features (SURF). *Computer Vision and Image Understanding*, **110**(3), 346–359, ISSN 1077-3142 (doi: 10.1016/j.cviu.2007.09.014)

Chan WS, Mah ML, Voight DE, Fitzpatrick JJ and Talghader JJ (2014) Crystal orientation measurements using transmission and backscattering. *Journal of Glaciology*, **60**(224), 1135–1139, ISSN 00221430 (doi: 10.3189/2014JoG14J071)

Craig JJ (2005) *Introduction to Robotics: Mechanics and Control*. Pearson Education, Upper Saddle River, NJ, 3 edition, ISBN 0-201-54361-3

Diprinzio CL, Wilen LA, Alley RB, Fitzpatrick JJ, Spencer MK and Gow AJ (2005) Fabric and texture at Siple Dome, Antarctica. *Journal of Glaciology*, **51**(173), 281–290

Doake CSM, Corr HFJ and Jenkins A (2002) Polarization of radio waves transmitted through Antarctic ice shelves. *Annals of Glaciology*, **34**, 165–170, ISSN 0260-3055, 1727-5644 (doi: 10.3189/172756402781817572)

Durand G, Gagliardini O, Thorsteinsson T, Svensson A, Kipfstuhl S and Dahl-Jensen D (2006) Ice microstructure and fabric: An up-to-date approach for measuring textures. *Journal of Glaciology*, **52**(179), 619–630 (doi: 10.3189/172756506781828377)

Fitzpatrick JJ, Voigt DE, Fegyveresi JM, Stevens NT, Spencer MK, Cole-Dai J, Alley RB, Jardine GE, Cravens ED, Wilen LA, Fudge T and McConnell JR (2014) Physical properties of the WAIS Divide ice core. *Journal of Glaciology*, **60**(224), 1181–1198, ISSN 00221430, 17275652 (doi: 10.3189/2014JoG14J100)

Fueten F (1997) A computer-controlled rotating polarizer stage for the petrographic microscope. *Computers & Geosciences*, **23**(2), 203–208, ISSN 0098-3004 (doi: 10.1016/S0098-3004(97)85443-X)

Gow AJ and Kohnen H (1979) The relationship of ultrasonic velocities to c-axis fabrics and relaxation characteristics of ice cores from Byrd Station, Antarctica. *Journal of Glaciology*, **24**(90), 147–153, ISSN 0022-1430, 1727-5652 (doi: 10.3189/S0022143000014702)

Gusmeroli A, Pettit EC, Kennedy JH and Ritz C (2012) The crystal fabric of ice from full-waveform borehole sonic logging. *Journal of Geophysical Research: Earth Surface*, **117**(F3), F03021, ISSN 2156-2202 (doi: 10.1029/2012JF002343)

Kluskiewicz D, Waddington ED, Anandakrishnan S, Voigt DE, Matsuoka K and McCARTHY MP (2017) Sonic methods for measuring crystal orientation fabric in ice, and results from the West Antarctic ice sheet (WAIS) Divide. *Journal of Glaciology*, **63**(240), 603–617, ISSN 0022-1430, 1727-5652 (doi: 10.1017/jog.2017.20)

Matsuoka K, Wilen L, Hurley SP and Raymond CF (2009) Effects of birefringence within ice sheets on obliquely propagating radio waves. *IEEE Transactions on Geoscience and Remote Sensing*, **47**(5), 1429–1443, ISSN 1558-0644 (doi: 10.1109/TGRS.2008.2005201)

Paterson WSB and Waddington ED (1984) Past precipitation rates derived from ice core measurements: Methods and data analysis. *Reviews of Geophysics*, **22**(2), 123–130, ISSN 1944-9208 (doi: 10.1029/RG022i002p00123)

Petit JR, Duval P and Lorius C (1987) Long-term climatic changes indicated by crystal growth in polar ice. *Nature*, **326**(6108), 62–64, ISSN 1476-4687 (doi: 10.1038/326062a0)

Petrenko VF and Whitworth RW (1999) *Physics of Ice*. Oxford University Press, Oxford, ISBN 0-19-851895-1

Pettit EC, Thorsteinsson T, Jacobson HP and Waddington ED (2007) The role of crystal fabric in flow near an ice divide. *Journal of Glaciology*, **53**(181), 277–288

Rigsby GP (1960) Crystal orientation in glacier and in experimentally deformed ice. *Journal of Glaciology*, **3**(27), 589–606, ISSN 0022-1430, 1727-5652 (doi: 10.3189/S0022143000023716)

Slawny KR, Johnson JA, Mortensen NB, Gibson CJ, Goetz JJ, Shturmakov AJ, Lebar DA and Wendricks AW (2014) Production drilling at WAIS Divide. *Annals of Glaciology*, **55**(68), 147–155 (doi: 10.3189/2014AoG68A018)

Voigt DE, Fitzpatrick JJ and Alley RB (2015) C-axis fabric from physical properties samples of the wais divide ice core. "`http://www.usap-dc.org/view/dataset/609605`"

Wilen L (2000) A new technique for ice-fabric analysis. *Journal of Glaciology*, **46**(152), 129–139 (doi: 10.3189/172756500781833205)

Wilen L, Diprinzio C, Alley R and Azuma N (2003) Development, principles, and applications of automated ice fabric analyzers. *Microscopy Research and Technique*, **62**(1), 2–18, ISSN 1059-910X, 1097-0029 (doi: 10.1002/jemt.10380)

Wilson CJL and Peternell M (2011) Evaluating ice fabrics using fabric analyser techniques in Sørsdal Glacier, East Antarctica. *Journal of Glaciology*, **57**(205), 881–894, ISSN 0022-1430, 1727-5652 (doi: 10.3189/002214311798043744)